P116 AN ANALYSIS OF TERMINAL DOPPLER WEATHER AND PHASED ARRAY RADAR VELOCITY AND REFLECTIVITY SIGNATURES OF THE 20 MAY 2013, MOORE, OKLAHOMA TORNADO

Vincent T. Wood[1], Pamela L. Heinselman[1], Rodger A. Brown[1],
David L. Priegnitz[2], Donald W. Burgess[2], and Christopher D. Karstens[2]

[1]NOAA/OAR/National Severe Storms Laboratory, Norman, Oklahoma,
[2]Cooperative Institute for Mesoscale Meteorological Studies (CIMMS), University of Oklahoma, Norman, Oklahoma

1. INTRODUCTION

On 20 May 2013 a supercell thunderstorm in central Oklahoma produced a tornado that developed west of Moore at 1956 UTC, and rapidly intensified to EF4 intensity three min later (Figs. 1 and 2). The deadly tornado eventually reached EF5 intensity, tearing through a heavily populated section of Moore, killing 24 people and injuring scores of others. The tornado existed for about 40 min over a 23-km path that was up to 1.7-km wide (Burgess et al. 2014) and followed a track roughly similar to the Bridge Creek-Moore tornado of 3 May 1999 (Burgess et al. 2002).

This preliminary study describes the evolution of the tornado using the Oklahoma City-Terminal Doppler Weather Radar (TOKC) located south of Moore and the NOAA National Weather Radar Testbed Phased-Array Radar (NWRT PAR; hereafter PAR) located in Norman. The objectives of the study are two-folded: (a) to analyze and compare the detailed high-resolution Doppler velocity and reflectivity signatures in and around the tornado, as viewed simultaneously from two different radars, and (b) to determine any relationship between the tornado's varying strength and core size (via Doppler rotational velocities and core diameters) and the ground damage path.

2. DATA SOURCES AND PROCESSING

2.1 TOKC and PAR Characteristics

Operated by the Federal Aviation Administration, TOKC is a C-band Terminal Doppler Weather Radar (TDWR) located in north-northwest Norman (Fig. 1). TOKC is strategically located 15.5 km southeast of Will Roger World Airport in Oklahoma City and is primarily used for detecting hazardous low-altitude wind shear (associated with convective storms) and facilitating warning of the shear in regions close to the airport. Situated about 6 km southeast of TOKC, the PAR is located in north Norman and is part of the broader multifunction phased-array radar initiative that is investigating the use of a single radar system to perform both weather and aircraft surveillance functions (Weber et al. 2007; National Academies 2008). Interested readers may refer to Zrnić et al. (2007) for a detailed technical description of the PAR and Heinselman et al. (2008) and Heinselman and Torres (2011) for high-temporal-resolution capabilities of the PAR.

Selected attributes of the TOKC and PAR are shown in Table 1. TOKC is a 5-cm wavelength radar, whereas the PAR is a 9.38-cm wavelength radar. TOKC's 8.2-m diameter parabolic antenna results in a 0.55º half-power beamwidth (BW, hereafter simply referred to as beamwidth). In contrast with the TOKC parabolic antenna, the PAR has a single flat-face phased-array antenna of the type that has been used for a number of years on U. S. Navy ships [this antenna is on loan from the Navy (Forsyth et al. 2005; Zrnić et al. 2007)]. The antenna is rotated to cover the 90º-wide sector of interest and then remains stationary during data collection until the storms of interest move toward the edge of the sector. The antenna consists of 4352 radiating elements that produce a half-power BW of 1.5º at broadside (i.e., when the beam is perpendicular to the array plane). The BW gradually increases to 2.1º at a $\pm$45º angle from broadside (Fig. 3). The azimuthal spacing is one-half of the BW, beginning with 0.75º and ending with 1.06º. The PAR used 50% azimuthal overlapping at all elevation angles, yielding a total of 109 beam positions at each elevation angle that were needed to cover the 90º azimuthal sector (Torres et al. 2013).

Although both TOKC and PAR utilized volume scan strategies (not shown), we focus on high-resolution evolution of the tornado sampled at the lowest elevation angle (0.5º). TOKC's 0.5º elevation angle was revisited every 30 sec to ~1 min. The PAR's lowest elevation angle of 0.5º was revisited every ~1 min (Heinselman et al. 2008; Heinselman and Torres 2011).

The locations of the TOKC and PAR gave them excellent vantage points from which to observe the tornado, which was within 15 km of both radars for its entire lifetime. As the tornado made its closest approach (5.4 km to TOKC and 10.8 km to PAR) at 2017 UTC, data were collected at heights as low as 50—100 m AGL.

3. DATA ANALYSIS

3.1 Damage Survey

Damage survey methodology (Burgess et al. 2014) and NWS damage assessment toolkit (Camp et al. 2014) were used to assess the EF-scale ratings (McDonald et al. 2004; WSEC 2006) within the tornado's path (Fig. 1). The ground surveys were aided by use of high-resolution aerial and satellite imagery of the tornado damage. The

Corresponding author address: Vincent T. Wood, National Severe Storms Laboratory, 120 David L. Boren Blvd., Norman, Oklahoma 73072, USA; e-mail: Vincent.Wood@noaa.gov

tornado damage track was used to superimpose the ratings on the high-resolution Doppler velocity and reflectivity measurements, as viewed concurrently from two different radars.

3.2 Radar Data

TOKC (PAR) data were processed between 1901 and 2100 (2000—2100) UTC, thus providing excellent radar data that were continuous during the tornado's life. The PAR was initially directed toward other supercells to the south and was directed toward the Moore tornado after it has already developed. Solo3 software, now in its third version (https://www.eol.ucar.edu/software/solo3) was used to edit the radar data (Oye et al. 1995). One of the limitations of the TOKC was that there is low velocity aliasing (e. g., Nyquist velocity of 16- to- 22 m s^{-1} shown in Table 1) in the data where there were high velocities in the vortex signature. At times this aliasing made it difficult to dealias the velocities properly. Time (height) continuity of vortex signatures including calculated Doppler rotational velocities and core diameters were examined between volume scans (elevation angles) to ensure that the signatures did not change drastically and unrealistically.

3.3 Non-objective Analysis

The two-dimensional contouring technique of Bourke (1987) was chosen for analysis, rather than an objective analysis scheme, because radar data are displayed in their original coordinate system (range, azimuth and elevation angle) without altering the peak Doppler velocity values. The extreme velocity values of the high-resolution TOKC and PAR data were preserved within and surrounding the vortex signature.

3.4 ArcGIS

TOKC and PAR data were imported into ArcGIS for enhanced visualization and interpretation (e.g., Karstens et al. 2013). To accomplish this task, the radar data were converted to a Climate and Forecast (CF) compliant NetCDF format for subsequent conversion to shapefile format. All of the radar data shapefiles were imported and appropriate color scales were applied to the data. In addition to the radar data, civil infrastructure (i.e., roads) and EF-scale damage contours from the tornado damage survey were displayed to enhance interpretation of the data at various viewing scales.

4. COMPARATIVE RESULTS

This section compares the evolution of high-resolution Doppler velocity and reflectivity data, as viewed simultaneously from the TOKC and PAR.

4.1 Signal Attenuation

Signal attenuation problems occur with short wavelength radar when the radar is used for severe storm identification and structure analysis (e.g., Johnson and Brandes 1987). The primary drawback of using TOKC's 5-cm wavelength is signal attenuation that is relatively larger than with a 10-cm wavelength radar, which prevents accurate precipitation estimation in heavy rain. Signal attenuation on the far side (west-northwest through northeast) of the tornado-producing supercell is evident by comparing observations from TOKC and PAR (Fig. 4). Signal attenuation, however, does not impact the Doppler velocity measurements as long as the received signal remains above the system noise level (Johnson and Brandes 1987). Due to the location of the supercell relative to the radar (i.e., no storms between it and the radar), the main feature of interest -- the tornadic vortex signature and the tornado signature (as will be shown in subsection 4.2) -- were not impacted by attenuation.

4.2 Doppler Rotational Velocity and Core Diameter

Meteorologists and automated algorithms measure the strength and size of a Doppler vortex signature by the velocity difference between the two peaks in the characteristic velocity couplet (e.g., Mitchell et al. 1998; Stumpf et al. 1998). Herein, the mean rotational velocity (V_{ROT}), independent of storm motion, is calculated as the average of extreme positive and negative Doppler velocity values across an estimated tornado core diameter (*CD*) at the center range (R_C) and height (Z_C) of the Doppler vortex signatures, as seen simultaneously from TOKC and PAR (Table 2). These estimates of V_{ROT} and *CD* should be compared separately to the EF-scale ratings because of the differences in resolution and range of the tornado from the radar. The V_{ROT} (*CD*) values measured by PAR are lower (larger) than those by TOKC not only because the PAR has a broader beam but also because PAR's range to the tornado center is up to twice TOKC's range to the center. Also, PAR's larger beamwidth contributes to the larger areal coverage of debris signatures within the hook echo in the reflectivity fields.

The presence of a *tornado signature* (TS) is evident in Figs. 5-8, whereas the presence of a *tornadic vortex signature* (TVS) is evident in Fig. 9. The TS is a vortex signature of extreme Doppler velocity values (of opposite sign) separated by a few beamwidths in the azimuthal direction that arises when the tornado is within a few kilometers of a Doppler radar and the tornado is larger than the radar beam (Brown et al. 1978; Brown 1998). In contrast, the TVS arises when the radar beam is wider than the tornado producing a vortex signature of degraded Doppler velocity extremes (of opposite sign) separated by about one beamwidth in the azimuthal direction (Brown et al. 1978).

Doppler velocity contours superimposed with the EF-ratings along the damage paths are plotted in Figs. 5—9. Most of the positive and negative Doppler velocity peaks were not at the same range because target motion in the tornado vortex was slightly divergent, owing to debris centrifuging (Dowell et al. 2005).

When the tornado was closest to the radars at 2017 UTC (Fig. 7), TOKC and PAR measured strongest rotational velocities exceeding 70 and 60 m s^{-1}, respectively, in the lowest 50—100 m AGL at a time when the tornado was intense. After 2017 UTC, the tornado began to shrink in size, decreasing from EF5 to EF2-damage before eventually dissipating after 2035 UTC. A compact swath of EF5 damage a few hundred meters west of Interstate 35 in Moore, which occurred at around 2023 UTC, is associated with the slowing of the tornado's ground-relative speed as it traced out a very small loop in its path (the cusp in the damage track in Fig. 1).

The tornado vortex's core size and rotational velocity strength may influence the width of the ground damage path. For example, the core radius at which most damaging winds occur may increase the damage path width at one time (Fig. 5) and decrease the width at another time (Fig. 7). Since only five key times of evolution are presented in this study, the comparison will be expanded to include the full data set (1-min updates rather than key times shown here).

5. SUMMARY DISCUSSION

The Newcastle-Oklahoma City-Moore, Oklahoma tornado afforded the opportunity to (a) document detailed information on the evolution of high-resolution Doppler velocity fields in and around the tornado using nearby TOKC and PAR, and (b) implement comparisons between a damage survey and Doppler velocity measurements. This preliminary study is part of our ongoing research to continue documentation of detailed information on the evolution of the high-resolution Doppler velocity and reflectivity fields surrounding the tornado at all elevation angles.

Acknowledgments. The authors appreciate the helpful comments on this manuscript provided by Terry Schuur of NSSL. We thank (a) David Bodine of Advanced Radar Research Center at the University of Oklahoma for processing the TOKC radar data, (b) Robin Tanamachi of NSSL for assisting in Solo3 radar data editing task, and (c) Jeff Brogden of NSSL for ingesting radar data in the DORADE format and converting them into WDSS-II netCDF files. John Cho, TOKC engineer, is acknowledged for providing the effective beamwidth of TOKC; Dan Berkowitz of Radar Operations Center (ROC) for providing terrain elevation and radar antenna elevation of TOKC. The authors thank (a) numerous people at the National Weather Center who tirelessly contributed to the tornado ground damage survey of 20 May 2013, and (b) Kiel Ortega of NSSL and Gabe Garfield of NWS for generously providing their photographs in Fig. 2.

7. REFERENCES

Bourke, P., 1987: CONREC – A Contouring Subroutine. [Available online at http://paulbourke.net/papers/conrec/]

Burgess, D. W., M. A. Magsig, J. Wurman, D C. Dowell, and Y. Richardson, 2002: Radar observations of the 3 May 1999 Oklahoma City tornado. *Wea. Forecasting,* **17,** 456-471.

Burgess, D., K. Ortega, G. Stumpf, G. Garfield, C. Karstens, T. Meyer, B. Smith, D. Speheger, J. Ladue, R. Smith, and T. Marshall, 2014: 20 May 2013 Moore, Oklahoma tornado: Damage survey and analysis. *Wea. Forecasting* (in press).

Brown, R. A., 1998: Nomogram for aiding the interpretation of tornadic vortex signatures measured by Doppler radar. *Wea. Forecasting,* **13,** 505-512.

Brown, R. A., L. R. Lemon, and D. W. Burgess, 1978: Tornado detection by pulsed Doppler radar. *Mon. Wea. Rev.,* **106,** 29-38.

Camp, J. P., L. P. Rothfusz, A. Anderson, D. Speheger, K. L. Ortega, and B. R. Smith, 2014: Assessing the Moore, Oklahoma (2013) tornado using the National Weather Service Damage Assessment Toolkit. Extended Abstract, *Special Symposium on Severe Local Storms: The Current State of the Science and Understanding Impacts.* 5 February, Atlanta, GA, Amer. Meteor. Soc., Boston, P830.

Dowell, D. C., C. R. Alexander, J. M. Wurman, and L. J. Wicker, 2005: Centrifuging of hydrometeors and debris in tornadoes: Radar-reflectivity patterns and wind-measurement errors. *Mon. Wea. Rev.,* **133,** 1501-1524.

Forsyth, D. E., and Coauthors, 2005: The National Weather Radar Testbed (phased array). Preprints, 32nd Conf. on Radar Meteorology, Albuquerque, NM, Amer. Meteor. Soc., CD-Rom, 12R.3.

Heinselman, P. L., and S. M. Torres, 2011: High-temporal-resolution capabilities of the National Weather Radar Testbed phased-array Radar. *J. Appl. Meteor. Climatol.,* **50,** 579-593.

Heinselman, P. L., D. L. Priegnitz, K. L. Manross, T. M. Smith, and R. W. Adams, 2008: Rapid sampling of severe storms by the National Weather Radar Testbed phased array radar. *Wea. Forecasting,* **23,** 808-824.

Johnson, B. C., and E. A. Brandes, 1987: Attenuation of a 5-cm wavelength radar signal in the Lahoma-Orienta storms. *J. Atmos. Oceanic Technol.,* **4,** 512–517.

Karstens, C. D., W. A. Gallus, Jr., B. D. Lee, and C. A. Finley, 2013: Analysis of tornado-induced tree fall using aerial photography from the Joplin, Missouri, and Tuscaloosa-Birmingham, Alabama, tornadoes of 2011. *J. Appl. Meteor. Climatol,* **52,** 1049-1068.

McDonald, J. R., G. S. Forbes, and T. P. Marshall, 2004: The enhanced Fujita (EF) scale. Preprints, *22nd Conf. on Severe Local Storms,* Hyannis, MA, Amer. Meteor. Soc., 3B.2. [Available online at http://ams.confex.com/ams/pdfpapers/81090.pdf]

Mitchell, E. D., S. V. Vasiloff, G. J. Stumpf, A. Witt, M. D. Eilts, J. T. Johnson, and K. W. Thomas, 1998: The National Severe Storms Laboratory tornado detection algorithm. *Wea. Forecasting,* **13,** 352-366.

National Academies, 2008: *Evaluation of the Multifunction Phased Array Radar Planning Process.* National Academy Press, 79 pp.

Oye, R., C. Mueller, and S. Smith, 1995: Software for radar translation, visualization, editing, and interpolation. Preprints, *27th Conf. on Radar Meteorology,* Vail, Colorado, Amer. Meteor. Soc., 359 - 361.

Stumpf, G. J., A. Witt, E. D. Mitchell, P. L. Spencer, J. T. Johnson, M. D. Eilts, K. W. Thomas, and D. W. Burgess, 1998: The National Severe Storms Laboratory mesocylone detection algorithm for the WSR-88D. *Wea. Forecasting,* **13,** 304-326.

Torres, S., R. Adams, C. Curtis, E. Forren, I. Ivić, D. Priegnitz, J. Thompson, and D. Warde, 2013: New weather-surveillance capabilities for NSSL's phased-array radar. Preprints, *29th Conf. on Environmental Information Processing Technologies*, Amer. Meteor. Soc., Austin, TX, 8.2.

Weber, M. E., J. Y. N. Cho, J. S. Herd, J. M. Flavin, W. E. Benner, and G. S. Torok, 2007: The next-generation multimission U. S. surveillance radar network. *Bull. Amer. Soc.,* **88,** 1739–1751.

WSEC, 2006: A recommendation for an enhanced Fujita scale (EF-scale). Wind Science and Engineering Center Tech. Rep., Texas Tech University, 15 pp + 3 appendices. [Available online at http://www.depts.ttu.edu/nwi/Pubs/FScale/EFScale.pdf]

Zrnić, D. S., J. F. Kimpel, D. E. Forsyth, A. Shapiro, G. Crain, R. Ferek, J. Heimmer, W. Benner, T. J. McNellis, and R. J. Vogt, 2007: Agile beam phased array radar for weather observations. *Bull. Amer. Soc.,* **88,** 1753-1766.

TABLE 1. Comparison of TOKC and PAR operating characteristics.

	TOKC	PAR
Antenna		
Transmitted Peak Power	250 kW	750 kW
Half-Power Beamwidth	0.55º	1.5º at broadside (0.0º) → 2.1º away from broadside (±45º)
Effective Beamwidth	1.2º	1.5º→2.1º
Power Gain	50 dB	39 dB
Minimum Elevation	0.5º	0.5º
Maximum Elevation	28.2º	52.9º
Maximum Rotation Rate	5 RPM	Electronic Scan
Transmitter		
Frequency	C Band (5.5-5.65 GHz)	S Band (3200 MHz)
Pulse Depth	150 m	249 m
Wavelength	5.0 cm	9.38 cm
Pulse Width	1.1 μsec	1.57 μsec
Max	1.1 μsec	4.70 μsec
Pulse Repetition Frequency	2000 (max)	1400
Polarization	Linear Horizontal	Vertical
Maximum Reflectivity Range	460 km	460 km
Minimum Unambiguous Range	90 km	115 km
Maximum Doppler Range	90 km	230 km
Azimuthal Resolution	1.0º	0.75º at broadside increases to 1.06º at ±45º
Sensitivity	0 dBZ at 190 km 1 m^2 at 460 km	0 dBZ at 190 km 1 m^2 at 460 km
Nyquist Velocity	16 → 22.4 m s^{-1}	29.3 m s^{-1}

TABLE 2. Near-synchronous times, maximum EF rating, rotational velocity (V_{ROT}), core diameter (CD), center range (R_C) and height (Z_C) to the Doppler vortex signature center, effective horizontal beamwidth (BW_E), vertical beamwidth (BW_V) as calculated and viewed near-simultaneously from TOKC and PAR (in parentheses) at 0.5^o elevation angle. The underlined numbers refer to the BW_E and BW_V that PAR would have had if it were located at the TOKC site. The asterisks indicate that the radar beam is wider than the tornado. PAR's BW_V and 0.5^o elevation angle are tilted 9.5^o from broadside (flat-face antenna is inclined at 10^o from vertical), as indicated by a dagger (†).

Time, UTC [hhmm:ss]	Max EF Rating	R_C [km]	Z_C [m, AGL]	BW_E [º, m, m]	BW_V [º, m, m]	V_{ROT} [m s^{-1}]	CD [m]
2003:00 (2003:09)	~EF3	9.08 (14.40)	83 (137)	1.2, 190 (1.87, 470, <u>296</u>)	0.55, 87 (1.52, 382, <u>241</u>)†	53 (40)	578 (948)
2009:58 (2009:50)	~EF4	6.83 (12.70)	61 (120)	1.2, 143 (1.51, 335, <u>180</u>)	0.55, 66 (1.52, 337, <u>181</u>)†	68 (48)	394 (595)
2017:35 (2017:22)	~EF5	5.40 (10.80)	48 (101)	1.2, 113 (1.50, 283, <u>141</u>)	0.55, 52 (1.52, 287, <u>143</u>)†	75 (62)	293 (430)
2025:55 (2025:34)	~EF4	7.35 (10.50)	67 (98)	1.2, 154 (1.51, 277, <u>194</u>)	0.55, 71 (1.52, 278, <u>195</u>)†	46 (37*)	261 (210*)
2035:00 (2035:09)	~EF2	12.23 (12.49)	116 (118)	1.2, 256 (1.51, 329, <u>322</u>)	0.55, 117 (1.52, 332, <u>325</u>)†	31* (25*)	266* (328*)

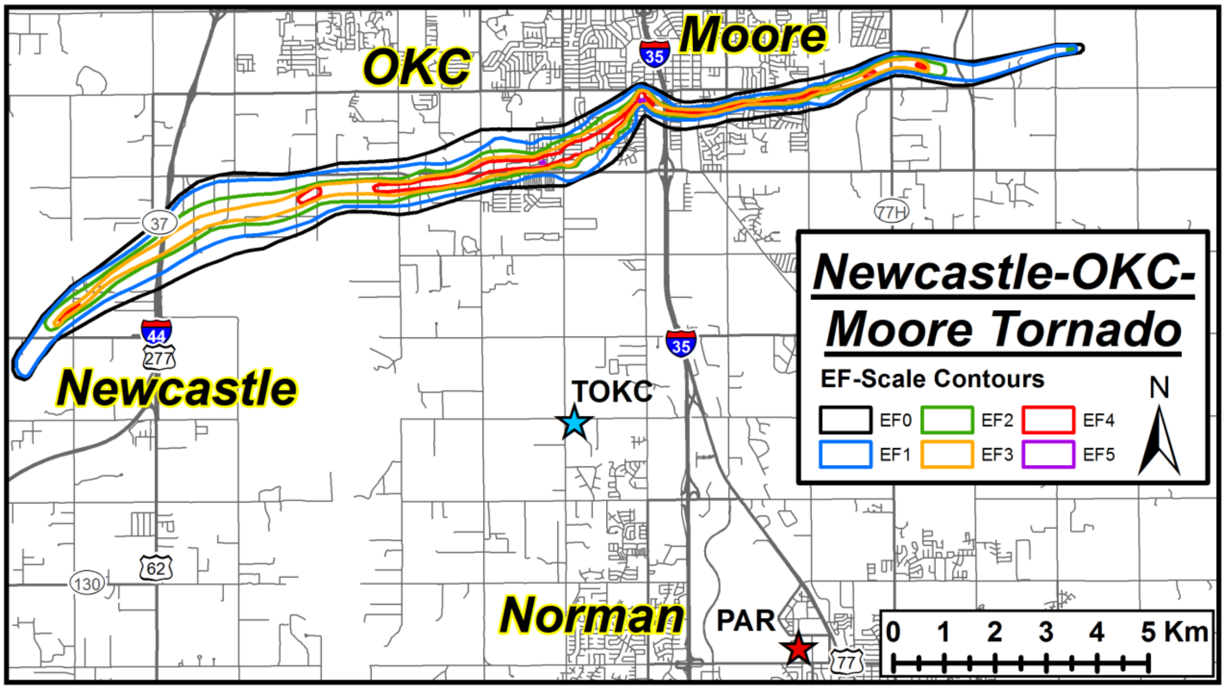

FIG. 1. Damage survey compiled by the National Weather Center teams for the Newcastle-Oklahoma City-Moore, Oklahoma tornado of (1956 – 2035 UTC) 20 May 2013. The EF-ratings along the damage path are contoured according to different colors. The blue (red) star shows the location of TOKC (PAR).

FIG. 2. The Newcastle-Oklahoma City-Moore tornado of 20 May 2013 at (a) 2003 UTC, (b) 2015-2020 UTC, and (c) 2019-2020 UTC. Photographs courtesy of K. Ortega and G. Garfield.

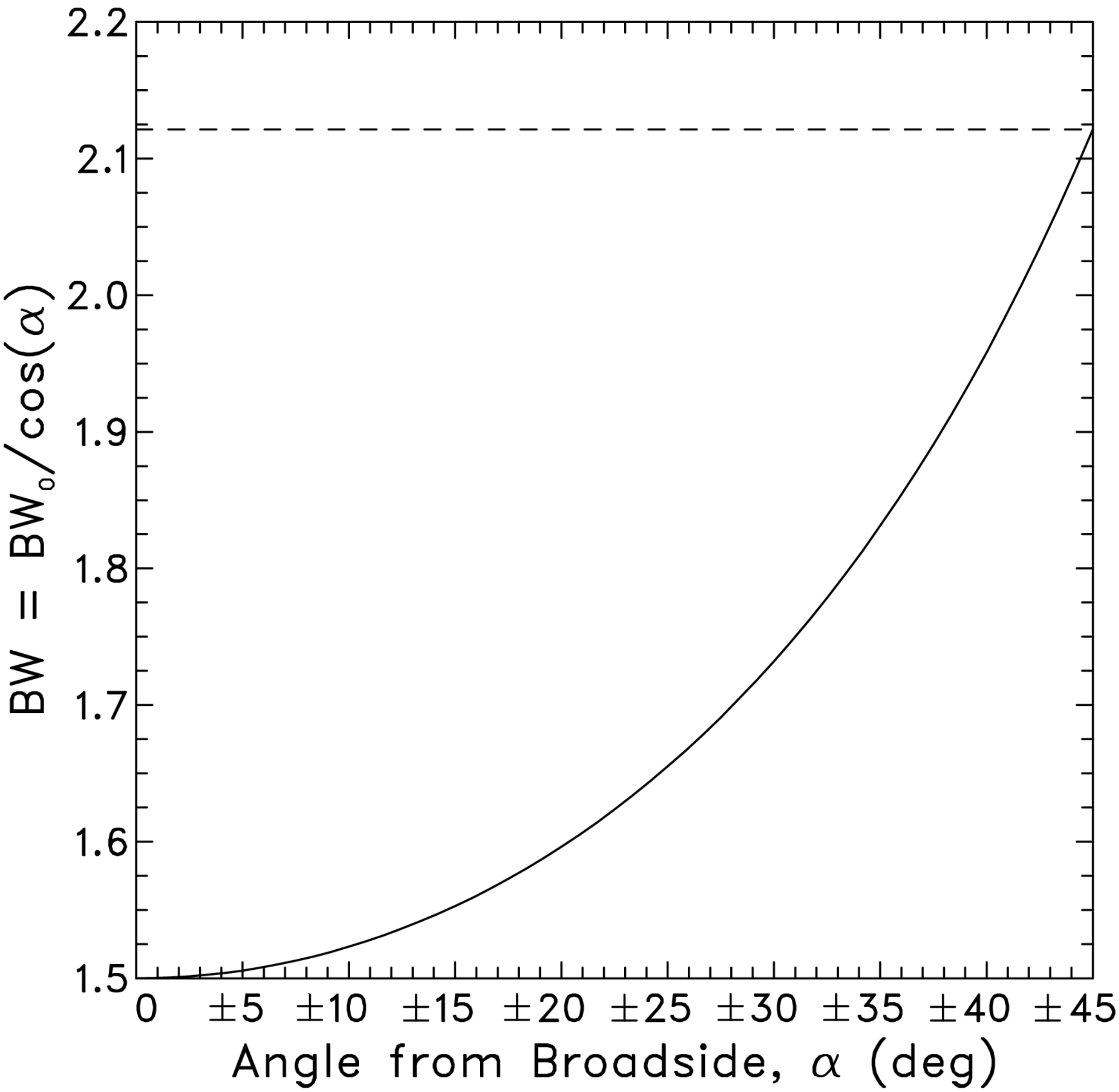

FIG. 3. PAR's effective horizontal beamwidth (BW) change in the azimuthal direction according to $BW_o/\cos(\alpha)$, where BW_o is the broadside BW and α is the azimuth angle relative to the broadside direction. The horizontal dashed line represents the upper limit at $\alpha = \pm 45^o$.

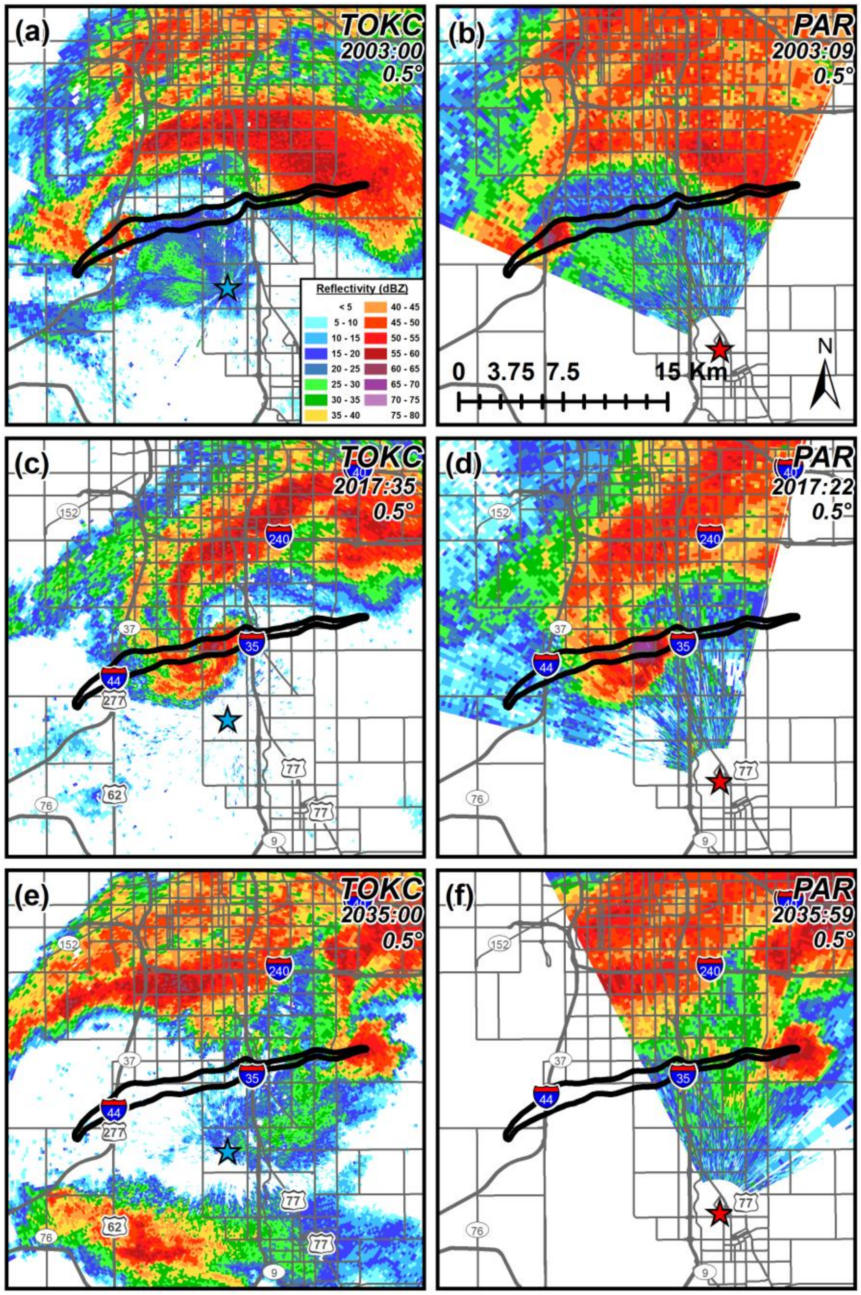

FIG. 4. Reflectivity fields as seen from TOKC (left 30-km x 30-km panels) and PAR (right 30-km x 30-km panels) at 0.5° elevation angle at (a) and (b) 2003 UTC, (c) and (d) 2017 UTC, and (e) and (f) 2035 UTC. The EF0 (black, thick curve) rating along the damage path is contoured. The blue (red) star shows the location of TOKC (PAR). Streets, highways and interstates are indicated.

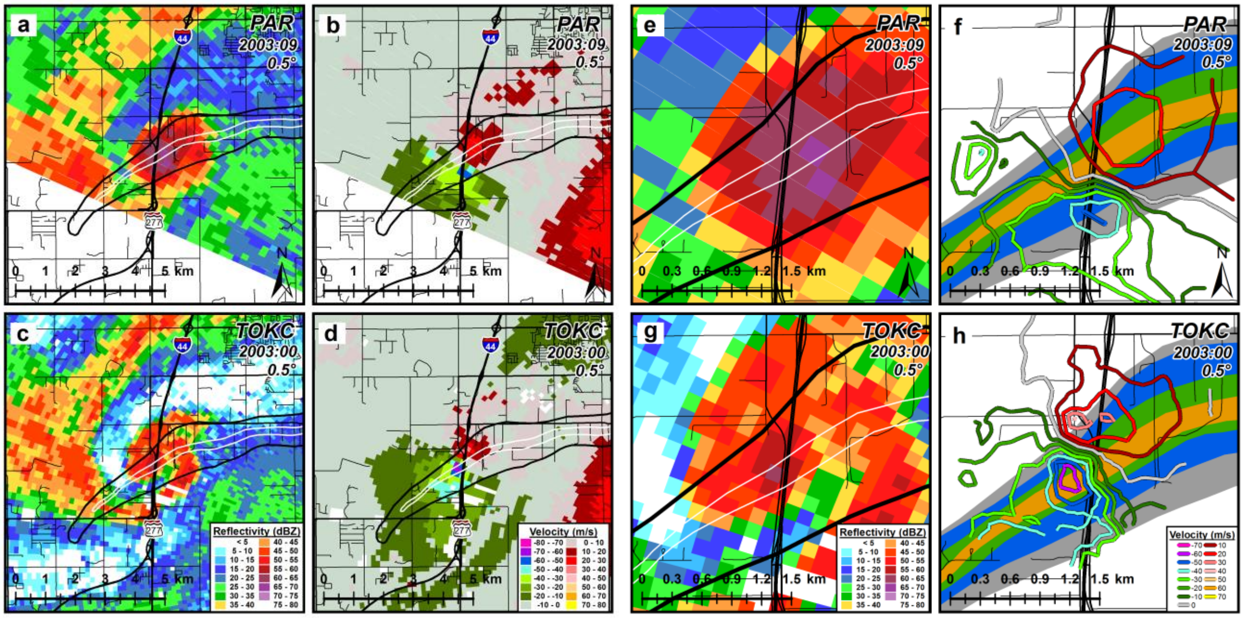

FIG. 5. (a), (c), (e) and (g) radar reflectivity (dBZ) and (b), (d), (f) and (h) ground-relative Doppler velocity (m s^{-1}) fields associated with the Moore tornado as seen simultaneously from PAR and TOKC (10-km x 10-km panels on the left and 3-km x 3-km panels on the right) at 0.5^o elevation angle at 2003 UTC. In (a)-(g), the EF0 (black) and EF3 (white) ratings along the damage path are contoured. In (f) and (h), colored Doppler velocity (ground-relative) contours are superimposed with the EF-ratings along the damage path. Streets, highways and interstates are indicated. The slight misalignments between the Doppler velocity measurements and the damage path apparently are due to slight ranging errors associated with PAR.

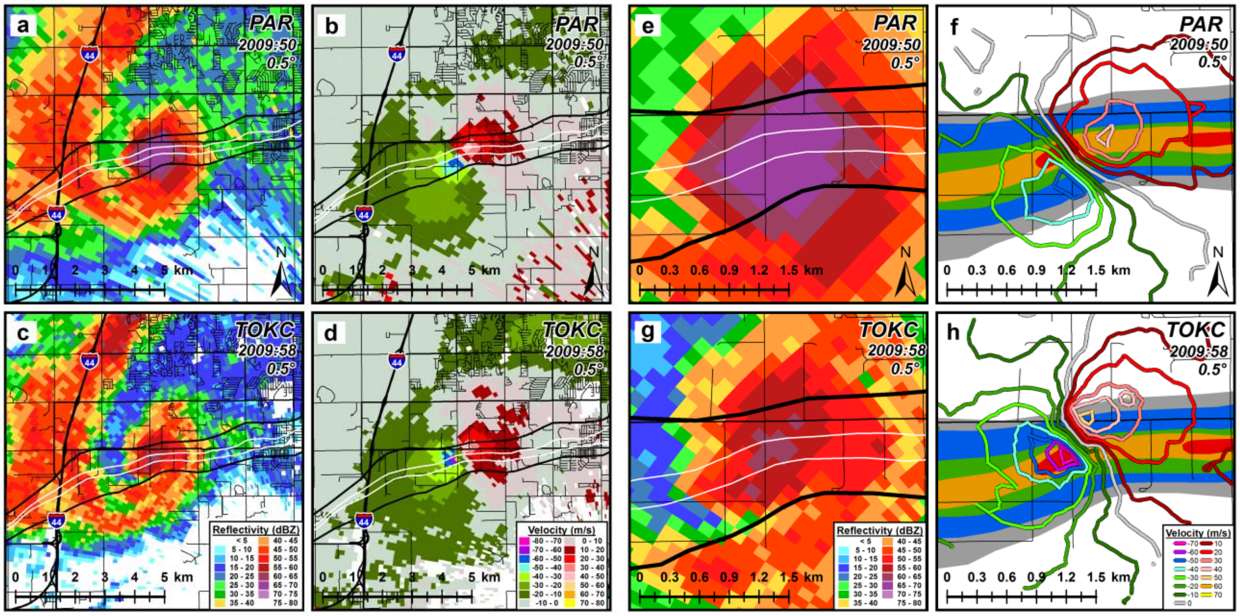

FIG. 6. Same as FIG. 5, except for 2009 UTC.

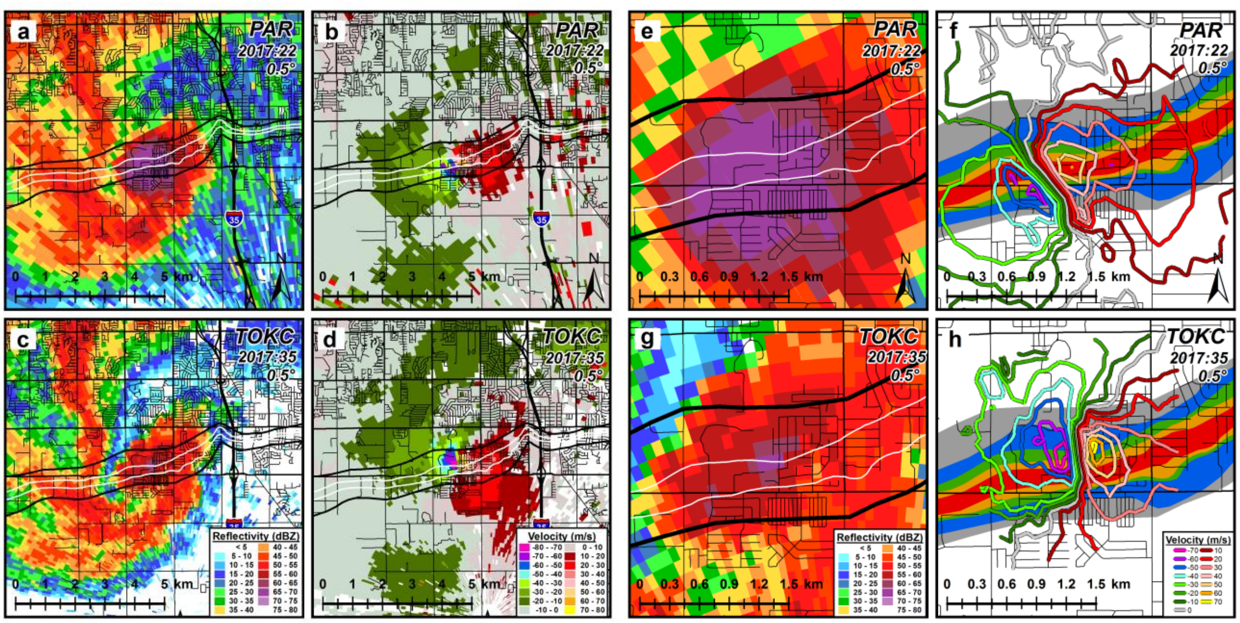

FIG. 7. Same as FIG. 5, except for 2017 UTC.

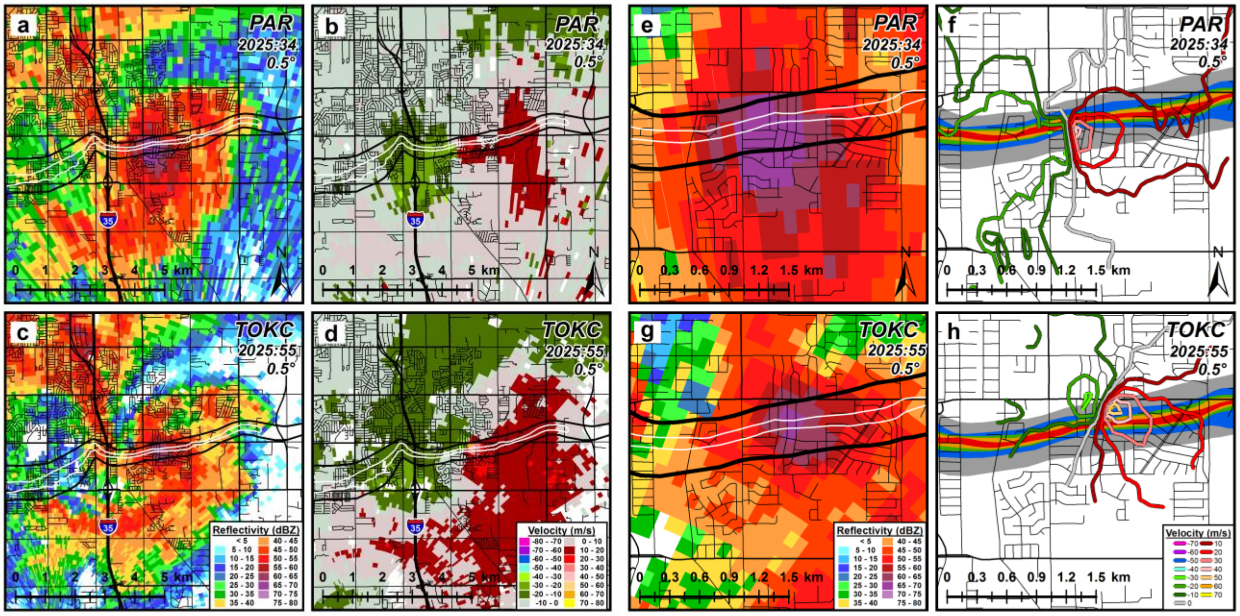

FIG. 8. Same as FIG. 5, except for 2025 UTC.

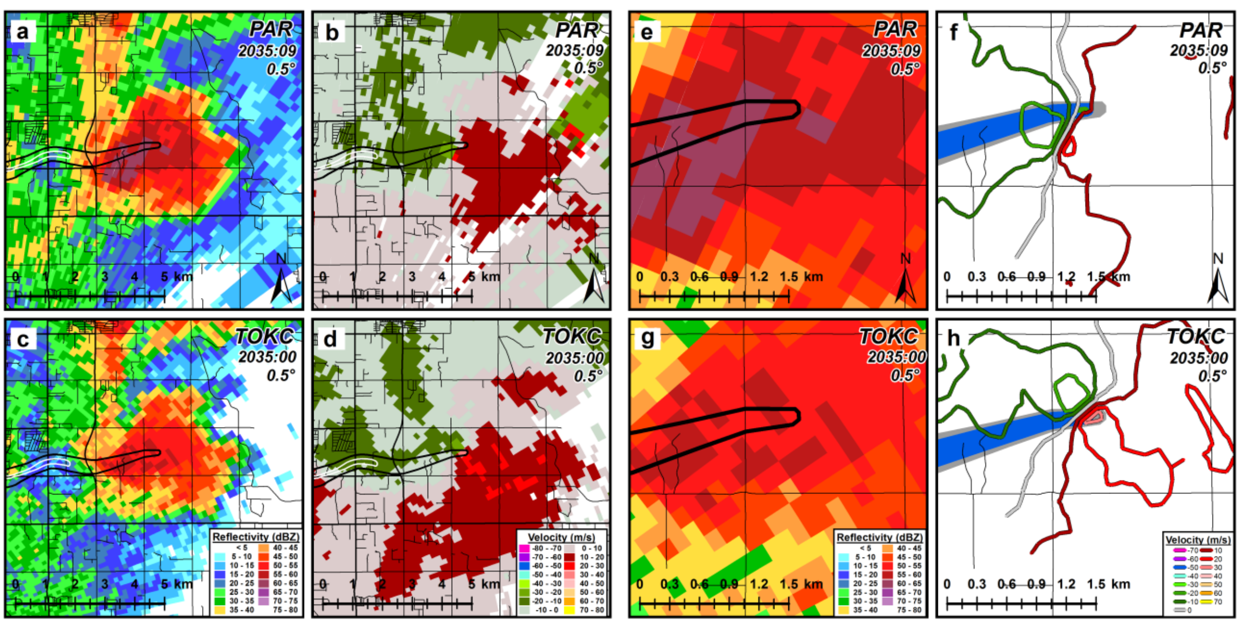

FIG. 9. Same as FIG. 5, except for 2035 UTC.